


Finite-temperature thermodynamic properties of spin-1 nematics in an applied magnetic field

Katsuhiko Tanaka and Chisa Hotta

Department of Basic Science, University of Tokyo, Meguro, Tokyo 153-8902, Japan

 (Received 28 April 2020; accepted 8 September 2020; published 5 October 2020)

We study numerically the thermodynamic properties of the spin nematic phases in a magnetic field in the spin-1 bilinear-biquadratic model. When the field is applied, the phase transition temperature initially goes up and then decreases rapidly toward zero, which is detected by the peak shift in the specific heat. The underlying mechanism of the reentrant behavior is the entropic effect. In a weak field the high temperature paramagnetic phase rapidly loses its entropy while the ferroquadrupolar nematic phase remains robust by modifying the shape of the ferroquadrupolar moment. This feature serves as a fingerprint of generic ferroquadrupolar phases, while it is not observed for the case of antiferroquadrupoles.

DOI: [10.1103/PhysRevB.102.140401](https://doi.org/10.1103/PhysRevB.102.140401)

Introduction. Among symmetry broken phases in solids, those of higher order multipolar degrees of freedom are hard to study and have been often referred to as “hidden orders.” This is because their order parameters are not linearly coupled to external fields or forces, and thus are extremely difficult to characterize by the conventional experimental probes, as well known in heavy fermion examples such as CeB₆ [1,2], URu₂Si₂ [3,4]. Still, making use of the coupling between wave function and the crystal lattice distortion, the electronic quadrupolar orderings in CeB₆ are detected by the elasticity measurements [5]. The elasto-resistivity measurements are also performed for the clarification of the orbital nematics in iron pnictide [6].

In quantum magnets, the quadrupolar orderings of localized spins are often referred to as spin nematics. Unlike the true hidden orders, the quadrupolar spin moments are already well defined in theories [7]. Nevertheless, the spin nematics are still “hidden” in the sense that they are often invisible to local magnetic probes such as neutron scattering or magnetic resonances and only show featureless paramagnetic-like responses to a static magnetic field. Efforts to measure the dynamical quantities have been made [8–23], e.g., in the nuclear magnetic resonance [10–14,16,21], and inelastic neutron scattering [17,19], or the electron spin resonance [20,22], while experiments and theories are difficult to reconcile.

Spin nematics can resort to Landau’s approaches on second-order phase transitions, where some anomalies are found in the magnetocaloric and ac magnetic susceptibility measurements [24–26]. In theories, finite-temperature phase diagrams of spin-1 nematics at zero field are studied for the square lattice [27,28] and the triangular lattice [29,30] by the quantum Monte Carlo (QMC) simulation, and for the triangular lattice by the semiclassical method [31]. However, the basic information on how the quadrupolar moments of spin-1 respond to a magnetic field, and how they modify the finite temperature properties remain unexplored.

In this paper, we examine this issue by applying the Monte Carlo simulations to the spin-1 bilinear-biquadratic (BLBQ)

model, a canonical model for spin nematics. A pure quantum quadrupole is represented by a director \mathbf{d} , a real vector pointing perpendicular to the fluctuating spin moments, which does not couple to a magnetic field. However, the imaginary component of \mathbf{d} relevant to the emergent dipole moment couples to the field, which modifies the shape of the quadrupole to those fluctuating in-plane [8]. Since this modification keeps the spin nematic state robust against the weak field, the transition temperature goes up slightly and then starts to decrease against a stronger field. The former behavior reminds us of the Pomeranchuk effect in ³He [32] whose liquid and solid phases may roughly correspond to our nematic and paramagnetic phases, respectively. In fact, the paramagnetic phase rapidly loses its entropy with an applied field and gives way to the nematic phase, just like decreasing the pressure in ³He will transform the solid to liquid by releasing the entropy. The reentrant effect is a general feature of the ferroquadrupolar nematic phase as it is observed also in a square lattice, whereas not in the antiferroquadrupolar phases.

Spin-1 bilinear-biquadratic model. We deal with the spin-1 BLBQ model on the triangular and square lattices in a magnetic field;

$$\mathcal{H} = \sum_{\langle i,j \rangle} [J\hat{S}_i \cdot \hat{S}_j + K(\hat{S}_i \cdot \hat{S}_j)^2] - h \sum_{i=1}^N \hat{S}_i^z, \quad (1)$$

where \hat{S}_i is the spin-1 operator on site- i with $i = 1-N$, and J , K , and h denote the Heisenberg (bilinear) and biquadratic (BQ) interactions, with the magnetic field applied parallel to the z axis, respectively. Hereafter, J and K are normalized as $J^2 + K^2 = 1$.

Semiclassical approaches using the variational method revealed that in the absence of a magnetic field, the ground state of Eq. (1) has a ferroquadrupolar (FQ) order for $K/J < \tan^{-1}(-2)$ with $J > 0$, or $K < J \leq 0$ for the triangular lattice, and $K < J < 0$ for the square lattice [8,33,34], which agree qualitatively well with those from the fully quantum approaches. When a magnetic field is applied along the z -axis,

the FQ state acquires a small but finite magnetic moment along the z -axis while retaining its quadrupolar moment in the xy -plane. It then finally turns into a fully polarized magnetic phase at $h = z(J - K)$, where z is the coordination number [8,33,35,36].

Monte Carlo method with semiclassical SU(3) approximation. We employ the semiclassical SU(3) approximation combined with classical Monte Carlo methods [sSU(3)-MC] [31]. The wave functions are approximated by the direct product form of the one-body wave functions as

$$|\Psi\rangle = \bigotimes_{i=1}^N |\psi_i\rangle, \quad |\psi_i\rangle = \sum_{\alpha=x,y,z} d_{i,\alpha} |\alpha\rangle_i, \quad (2)$$

where $d_{i,\alpha}$ is the complex coefficient satisfying $|d_i| = 1$. The time-reversal invariant basis states $|\alpha\rangle$ are given as

$$|x\rangle = \frac{i(|+1\rangle - |-1\rangle)}{\sqrt{2}}, \quad |y\rangle = \frac{|+1\rangle + |-1\rangle}{\sqrt{2}}, \quad |z\rangle = -i|0\rangle, \quad (3)$$

where $|n\rangle$ ($n = 0, \pm 1$) is the spin-1 state with $S^z = n$. The energy evaluated using this wave function, $E_{\text{sSU}(3)} = \langle \Psi | \mathcal{H} | \Psi \rangle$, is given as

$$E_{\text{sSU}(3)} = \sum_{\langle i,j \rangle} [J \mathbf{d}_i^* \cdot \mathbf{d}_j]^2 + (K - J) |\mathbf{d}_i \cdot \mathbf{d}_j|^2 + ih \sum_{i=1}^N (\mathbf{d}_i^* \times \mathbf{d}_i)^z + \text{const.} \quad (4)$$

A set of parameters $\{d_{i,\alpha}\}_{i=1,\dots,N}$ is updated by the standard classical MC sampling with the canonical ensemble of $\exp(-\beta E_{\text{sSU}(3)})$, where $\beta = (k_B T)^{-1}$ is the inverse temperature. The spin moment whose z component appears in the Zeeman term of Eq. (4) is given explicitly as

$$\mathbf{S}_i = \langle \psi_i | \hat{\mathbf{S}}_i | \psi_i \rangle = -i \begin{pmatrix} d_{i,y}^* d_{i,z} - d_{i,z}^* d_{i,y} \\ d_{i,z}^* d_{i,x} - d_{i,x}^* d_{i,z} \\ d_{i,x}^* d_{i,y} - d_{i,y}^* d_{i,x} \end{pmatrix}. \quad (5)$$

The spin quadrupolar operator, $\hat{Q}_i^{\alpha\beta} = \hat{S}_i^\alpha \hat{S}_i^\beta + \hat{S}_i^\beta \hat{S}_i^\alpha - 2S(S+1)/3\delta_{\alpha\beta}$, is a rank-2 traceless symmetric tensor, and its vector representation for five linearly independent components, $\hat{Q}_i = (\hat{Q}_i^{x^2-y^2}, \hat{Q}_i^{3z^2-r^2}, \hat{Q}_i^{xy}, \hat{Q}_i^{yz}, \hat{Q}_i^{zx})$, is generally applied, which are evaluated as

$$\mathbf{Q}_i = \langle \psi_i | \hat{Q}_i | \psi_i \rangle = \begin{pmatrix} -(|d_{i,x}|^2 - |d_{i,y}|^2) \\ -\frac{1}{\sqrt{3}}(2|d_{i,z}|^2 - |d_{i,x}|^2 - |d_{i,y}|^2) \\ -(d_{i,x}^* d_{i,y} + d_{i,y}^* d_{i,x}) \\ -(d_{i,y}^* d_{i,z} + d_{i,z}^* d_{i,y}) \\ -(d_{i,z}^* d_{i,x} + d_{i,x}^* d_{i,z}) \end{pmatrix}. \quad (6)$$

Our simulation is performed on the lattice of $N = L \times L$, with $L = 12-36$ and $L = 8-32$ for the triangular and square lattices, respectively, under the periodic boundary condition. We combine the conventional Metropolis method with single spin rotations and replica exchange method [37], taking averages over the independent initial configurations using the jackknife

resampling. Each run consisting of 10^6-10^7 MC steps for thermalization and measurements, respectively.

The sSU(3)-MC considers only the leading terms of the cumulant expansion of the partition function [31], which nevertheless incorporates an amount of quantum and thermal fluctuations far beyond the simple mean-field calculation [38]. In fact, Eq. (2) describes well the nematic ground states of spin-1 BLBQ models [8,33,34]. At finite temperature, the stochastic MC averages further allows us to include the spatial fluctuation effect intrinsic to the second order phase transition. In the same context, the sSU(3)-MC has distinct advantages over the simple classical approximation which treats the spin moments as vectors [39]; in our case the vector \mathbf{d}_i represents the quantum quadrupole or the local quantum entanglement which orders by the BQ interaction, whereas the same interaction in the classical method favors the collinear spin orderings [31].

An artifact of adopting the formally classical Hamiltonian Eq. (4) is the lack of quantum condensation at low temperature; the T^2 -dependent specific heat characterizing the lowest energy excitations of three-colored Schwinger bosons of the spin-1 BLBQ model [8,33,40] is not observed [41]. However, in the temperature range of our focus, such behavior is easily wiped out by the thermal fluctuations and the collective behavior of quadrupoles become dominant, where the validity of Eq. (4) shall be recovered. In fact, the previous QMC calculations show that the specific heat deviates from T^2 at $T \sim T_c/2$ [29,30].

Ferroquadrupolar phase. We first present the finite-temperature properties of the FQ states. Fig. 1(a) shows the $T-h$ phase diagram for the triangular lattice at $(J, K) = (0, -1)$ where the ground state has a FQ ordering. We determine the transition temperature T_c as the peak position of the specific heat C/N ; Fig. 1(b) shows the temperature dependence of C/N in various magnetic fields. The peak position first slightly shifts to higher temperature and at $h \gtrsim 1$ starts to move rapidly toward lower temperature. We compare the results of $L = 12$ and 36 to show that the finite size effects are small enough, where T_c is always slightly lower and the peak height increases for larger L for all values of h we examined. To understand this reentrant behavior of T_c , we analyze the T dependence of the entropy density $\tilde{s}(T, h)$ and the energy density $e(T, h)$ in a weak field as shown in Figs. 1(c) and 1(d) [41]; $\tilde{s}(T, h)$ does not change much with h for the FQ phase. In contrast, the paramagnetic phase rapidly loses its entropy with h since the magnetic moment starts to align in the same direction. Since h gives a nearly constant shift in the energy $e(T, h)$ common to both phases, which is dominated by the Zeeman term, the reentrant behavior is understood as an entropic effect.

Figures 1(e) and 1(f) show the magnetic susceptibilities of the spin component perpendicular and parallel to the magnetic field, $\chi^\perp = (\chi^x + \chi^y)/2$, and χ^z , respectively, where $\chi^\alpha = \beta N (\langle (S^\alpha)^2 \rangle - \langle S^\alpha \rangle^2)$. One finds that χ^z starts to develop a small peak at T_c when h is applied, indicating that the finite magnetic moment is induced along the z -axis. The value of χ^\perp remains almost featureless, but a small structure appears at the same position as χ^z for larger L . The magnetization $\langle S^z \rangle$ does not depend much on T and its value in the FQ phase is in good

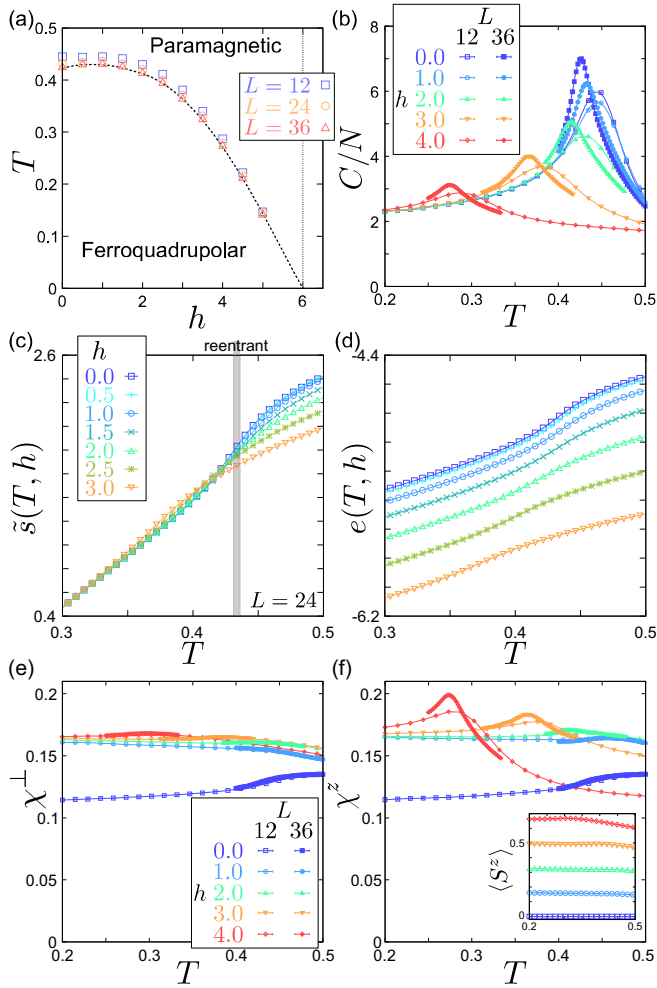


FIG. 1. Results of the sSU(3)-MC simulations on the triangular lattice at $(J, K) = (0, -1)$. (a) T - h Phase diagram. Squares, circles, and triangles are the peak positions of the specific heat estimated by the Gaussian kernel approximation in $L = 12, 24, 36$ samples, respectively. (b) Temperature dependence of the specific heat C/N for the various values of magnetic field h in $L = 12$ (open) and 36 (solid) samples. (c), (d) Temperature dependence of the entropy $\tilde{s}(T, h)$ and energy $e(T, h)$ per site in an $L = 24$ sample. (e), (f) Temperature dependence of the magnetic susceptibilities perpendicular and parallel to the magnetic field for the various values of h , in $L = 12$ (open) and 36 (solid) samples. The inset in (f) is the temperature dependence of the averaged magnetization density for $L = 12$.

agreement with the ground state ones, $m = h/[6(J - K)] = h/6$ (see inset of Fig. 1(f)) [8,33].

We next examine the field-dependence of the quadrupolar moments. In the ground state, the magnetic field confines the \mathbf{d} -vector within the xy -plane, namely, $|\Psi\rangle = \bigotimes_{i=1}^N |\mathbf{d}_i\rangle$ with $|\mathbf{d}_i\rangle = d_x |x\rangle + d_y |y\rangle$. This is because h couples to $d_x^* d_y - d_y^* d_x$ but not with d_z [see Eq. (4)] [8,33]. When \mathbf{d} is real, a pure quadrupole is formed $O(2)$ -symmetric about the director \mathbf{d} , as shown in the first column of Fig. 2(a). At $h \neq 0$ the emergent imaginary component of \mathbf{d} will distort it by shifting its fluctuation center toward the $+z$ -direction [33] [see the second and third columns of Fig. 2(a)].

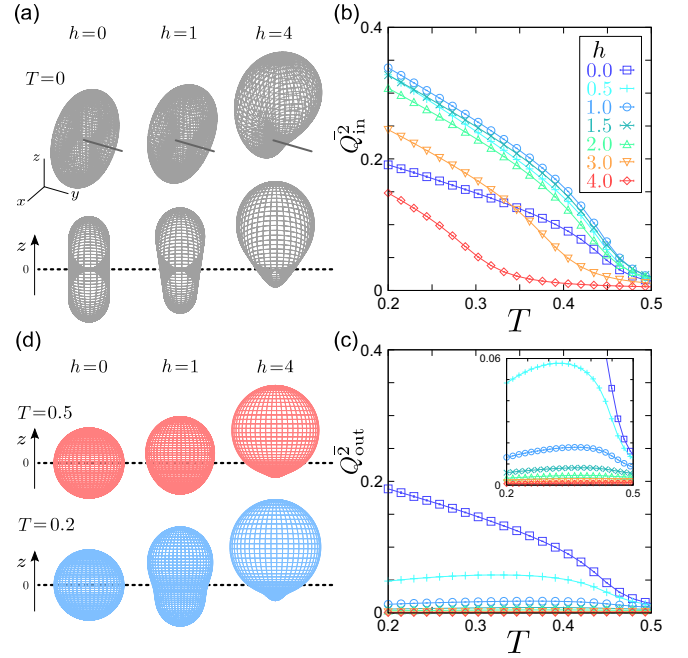


FIG. 2. (a) Spin-component distributions for the states at $T = 0$ in a magnetic field where $\mathbf{d} \in \mathbb{R}$ (bold line) is pointing in the y direction. The lower panel is the view in the x -direction. (b), (c) Temperature dependence of (b) \bar{Q}_{in}^2 and (c) \bar{Q}_{out}^2 [Eq. (7)] in the $L = 12$ triangular lattice. The inset in (c) is the enlarged view in the small \bar{Q}_{out}^2 region. (d) Spin-component distributions for the states evaluated by the sSU(3)-MC at $T \neq 0$ and $h = 0, 1, 4$ in $L = 12$ triangular lattice, viewed perpendicular to the z -axis. The upper/lower panels belong to the paramagnetic/FQ phases. Since the calculation does not break the $O(2)$ symmetry about the z -axis, the quadrupolar moments of $T = 0.2$ ones are the averages of those of the symmetry broken ones with its director pointing in a particular direction, which is also consistent with the Mermin-Wagner theorem.

The relationship between \mathbf{d} and the shape of the quadrupole is understood more clearly from Eq. (6) as follows; when d_z is zero so do $\langle Q^{yz} \rangle$ and $\langle Q^{zx} \rangle$, while $\langle Q^{x^2-y^2} \rangle$ and $\langle Q^{xy} \rangle$ which consist only of x and y elements of \mathbf{d} can respond to h . Based on this consideration, we define two kinds of squared quadrupolar moments,

$$\begin{aligned} \bar{Q}_{\text{in}}^2 &= \frac{1}{2}[(Q^{x^2-y^2})^2 + (Q^{xy})^2], \\ \bar{Q}_{\text{out}}^2 &= \frac{1}{2}[(Q^{yz})^2 + (Q^{zx})^2], \end{aligned} \quad (7)$$

where we straightforwardly find $\bar{Q}_{\text{in}}^2 \neq 0$ and $\bar{Q}_{\text{out}}^2 = 0$ at $T = 0$ and $h \neq 0$.

Temperature dependences of \bar{Q}_{in}^2 and \bar{Q}_{out}^2 are shown in Figs. 2(b) and 2(c). In a weak field, \bar{Q}_{in}^2 first increases and then at around $h \gtrsim 1$ starts to decrease with h . Whereas, \bar{Q}_{out}^2 takes a small but finite value at small h and $T \neq 0$ because of the thermal fluctuation, and becomes $\bar{Q}_{\text{out}}^2 = 0$ at $T = 0$. Notice that the apparently large values of \bar{Q}_{out}^2 at $h = 0$ occur simply because the moments are decoupled to the spatial coordinate. Once the field increases to $h \gtrsim 1$, \bar{Q}_{out}^2 is suppressed to zero for all temperatures. These results indicate that there

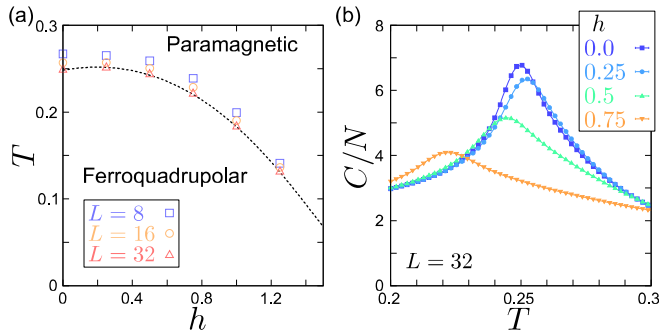


FIG. 3. (a) T - h phase diagram and (b) the T -dependence of C/N for the square lattice at $K/J = 2$ with $J, K < 0$.

is a crossover at $h \sim 1$ from the low-field regime with a robust quadrupolar moment to the high field regime where the quadrupolar moment is rapidly suppressed with field. It apparently links with the reentrant behavior of T_c at $h \lesssim 1$. Such particular field-dependence of the quadrupolar moment is visualized in Fig. 2(d). Compared to the ones at $T = 0$, the quadrupoles at $h = 1$ and $T = 0.2$ have a gourd-shape which indicates that \mathbf{d} cants slightly off the xy -plane to maximize the fluctuation.

Remarks. The geometry of the lattice does not seem to play any intrinsic role. As shown in Figs. 3(a) and 3(b), we also perform a similar calculation for the square lattice at $K/J = 2$ with $J, K < 0$ [43], finding a reentrant behavior at $h \lesssim 0.25$ [41].

In both Eqs. (1) and (4), the continuous symmetry exists, in which case a bulk finite-temperature phase transition is prohibited by the Mermin-Wagner theorem [44]. However, the specific heat shows a peak at T_c not only in our case but in the previous QMC calculations, which indicates the development of an intrinsic quasi-long-range ordering [45]. The growth of correlation length at T_c , even if it does not diverge, will drive the system to a long-range ordering once we stack the two-dimensional layer and include the interlayer coupling, which is the situation expected for the actual material systems.

Antiferroquadrupolar phase. Finally, we briefly discuss the finite-temperature properties and field dependence for the antiferroquadrupolar (AFQ) phase. In the ground state of the triangular lattice, the AFQ is realized at $0 < J < K$ [8–10]. The quadrupole moments form a three-sublattice structure described by $|\Psi\rangle = \bigotimes_{i=1}^{N/3} (|\mathbf{d}_{i_A}\rangle \otimes |\mathbf{d}_{i_B}\rangle \otimes |\mathbf{d}_{i_C}\rangle)$, where i_γ ($\gamma = A, B, C$) denotes the lattice sites with sublattice indices. At $h \neq 0$ and $T = 0$, the spatial direction of \mathbf{d}_{i_γ} is fixed, and two of three components, $|\mathbf{d}_{i_A}\rangle = |x\rangle$ and $|\mathbf{d}_{i_B}\rangle = |y\rangle$, behave similarly to the \mathbf{d} -vector of the FQ phase in a magnetic field, i.e., d_x and d_y become complex numbers, while $|\mathbf{d}_{i_C}\rangle = |z\rangle$ remains real [8]. Figure 4(a) shows the T - h phase diagram; T_c decreases with increasing h , which can be detected clearly by the temperature dependence of the specific heat in Fig. 4(b) for the different values of h in $L = 12$ and 36 samples. Although the quadrupoles on the A- and B-sublattices behave similar to that of the FQ phase, the difference lies in that they do not acquire a finite d_z and continue pointing within the xy -plane. In fact, the slight increase in T_c at small h is not

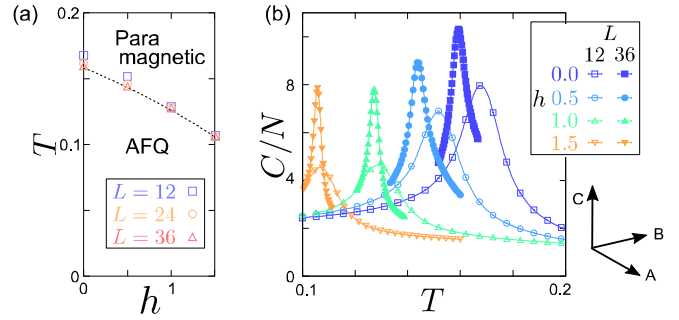


FIG. 4. (a) T - h phase diagram and (b) the T -dependence of C/N for the triangular lattice with $L = 12$ (open) and 36 (solid). The antiferroquadrupolar phase at $K/J = 2$ with $J, K > 0$ is studied [42], where A and B-sublattices gradually develop a magnetic moment similarly to that of the aforementioned FQ phase at $T = 0$. In the higher-field range of $h = 3/\sqrt{5} \approx 1.34$ to $3(1 - 1/\sqrt{5}) \approx 1.658$ a $2/3$ plateau phase appears, where the $|\mathbf{d}_{i_C}\rangle = |z\rangle$ remains and the spins on A and B sublattices are fully polarized.

observed in the case of AFQ. This is because the correlation between the quadrupoles of different sublattices do not allow the directors to cant off the original angle. The reentrant T_c is thus not observed for translational symmetry breaking AFQ ordering.

Conclusion. We disclosed the slight reentrant behavior of the paramagnetic-to-ferroquadrupolar spin nematic transition temperature in a weak magnetic field. Although both phases develop almost the same amount of magnetic moment by the field, only the nematic phase remains robust by modifying the shape of the quadrupolar moment toward the in-plane direction, and the counterpart paramagnet rapidly loses its entropy. One finds a common feature in ^3He in that the entropies of solid and liquid phases comes from the weakly interacting spin-1/2 nuclei and the condensed liquid of spins, respectively, although in their case the two phases are separated by the first order transition. If we regard the enthalpy $+PV$ as our Zeeman term, $-\langle S^z \rangle h$, the Pomeranchuk effect (^3He is cooled by tracing the solid-to-liquid transition temperature in applying the pressure) would explain our increase of T_c with h . In both cases, the decrease of relative entropy per unit (volume or spin) of solid to liquid plays a crucial role to raise T_c . A similar field reentrant phase diagram is found in the UUD plateau phase of the triangular lattice quantum magnet, where a large quantum fluctuation supported by the geometrical frustration shall play a similar role to our quadrupolar fluctuation [46]. We thus conclude that the present phenomenon not only serves as a clue to explore elusive nematic phase, but adds to the list of universal entropic effect intrinsic to the physics of quantum liquid versus paramagnet.

Acknowledgments. We thank Hikomitsu Kikuchi, Yutaka Fujii, Karlo Penc, Katsuhiko Morita, and Tsutomu Momoi for fruitful discussions and comments. This work is supported by JSPS KAKENHI Grants No. JP17K05533, No. JP18H01173, No. JP17K05497, and No. JP17H02916. Part of the calculations is done using the facilities of the Supercomputer Center, Institute for Solid State Physics, University of Tokyo.

- [1] J. Effantin, J. Rossat-Mignod, P. Burlet, H. Bartholin, S. Kunii, and T. Kasuya, *J. Magn. Magn. Mater.* **47-48**, 145 (1985).
- [2] T. Tayama, T. Sakakibara, K. Tenya, H. Amitsuka, and S. Kunii, *J. Phys. Soc. Jpn.* **66**, 2268 (1997).
- [3] W. Buyers, *Physica B* **223-224**, 9 (1996).
- [4] N. Shah, P. Chandra, P. Coleman, and J. A. Mydosh, *Phys. Rev. B* **61**, 564 (2000).
- [5] O. Suzuki, T. Goto, S. Nakamura, T. Matsumura, and S. Kunii, *J. Phys. Soc. Jpn.* **67**, 4243 (1998).
- [6] H.-H. Kuo, M. C. Shapiro, S. C. Riggs, and I. R. Fisher, *Phys. Rev. B* **88**, 085113 (2013).
- [7] A. F. Andreev and I. A. Grishchuk, *Sov. Phys. JETP* **60**, 267 (1984) [*Zh. Eksp. Teor. Fiz.* **87**, 467 (1984)].
- [8] A. Läuchli, F. Mila, and K. Penc, *Phys. Rev. Lett.* **97**, 087205 (2006).
- [9] H. Tsunetsugu and M. Arikawa, *J. Phys. Soc. Jpn.* **75**, 083701 (2006).
- [10] H. Tsunetsugu and M. Arikawa, *J. Phys.: Condens. Matter* **19**, 145248 (2007).
- [11] M. Sato, T. Momoi, and A. Furusaki, *Phys. Rev. B* **79**, 060406(R) (2009).
- [12] D. Podolsky and Y. B. Kim, *Phys. Rev. B* **79**, 140402(R) (2009).
- [13] M. Sato, T. Hikihara, and T. Momoi, *Phys. Rev. B* **83**, 064405 (2011).
- [14] M. Sato, T. Hikihara, and T. Momoi, *J. Phys.: Conf. Ser.* **320**, 012014 (2011).
- [15] R. Shindou, S. Yunoki, and T. Momoi, *Phys. Rev. B* **87**, 054429 (2013).
- [16] K. Nawa, M. Takigawa, M. Yoshida, and K. Yoshimura, *J. Phys. Soc. Jpn.* **82**, 094709 (2013).
- [17] A. Smerald and N. Shannon, *Phys. Rev. B* **88**, 184430 (2013).
- [18] O. A. Starykh and L. Balents, *Phys. Rev. B* **89**, 104407 (2014).
- [19] A. Smerald, H. T. Ueda, and N. Shannon, *Phys. Rev. B* **91**, 174402 (2015).
- [20] S. C. Furuya, *Phys. Rev. B* **95**, 014416 (2017).
- [21] A. Orlova, E. L. Green, J. M. Law, D. I. Gorbunov, G. Chanda, S. Krämer, M. Horvatić, R. K. Kremer, J. Wosnitza, and G. L. J. A. Rikken, *Phys. Rev. Lett.* **118**, 247201 (2017).
- [22] S. C. Furuya and T. Momoi, *Phys. Rev. B* **97**, 104411 (2018).
- [23] F. B. Ramos, S. Eliëns, and R. G. Pereira, *Phys. Rev. B* **98**, 094431 (2018).
- [24] B. Schmidt, P. Thalmeier, and N. Shannon, *Phys. Rev. B* **76**, 125113 (2007).
- [25] Y. Kohama, H. Ishikawa, A. Matsuo, K. Kindo, N. Shannon, and Z. Hiroi, *Proc. Natl. Acad. Sci. USA* **116**, 10686 (2019).
- [26] M. Skoulatos, F. Rucker, G. J. Nilsen, A. Bertin, E. Pomjakushina, J. Ollivier, A. Schneidewind, R. Georgii, O. Zaharko, L. Keller, C. Rüegg, C. Pfleiderer, B. Schmidt, N. Shannon, A. Kriele, A. Senyshyn, and A. Smerald, *Phys. Rev. B* **100**, 014405 (2019).
- [27] K. Harada and N. Kawashima, *J. Phys. Soc. Jpn.* **70**, 13 (2001).
- [28] K. Harada and N. Kawashima, *Phys. Rev. B* **65**, 052403 (2002).
- [29] R. K. Kaul, *Phys. Rev. B* **86**, 104411 (2012).
- [30] A. Völl and S. Wessel, *Phys. Rev. B* **91**, 165128 (2015).
- [31] E. M. Stoudenmire, S. Trebst, and L. Balents, *Phys. Rev. B* **79**, 214436 (2009).
- [32] I. Pomeranchuk, *Zh. Eksp. Teor. Fiz.* **20**, 919 (1950).
- [33] K. Penc and A. M. Läuchli, Spin nematic phases in quantum spin systems, in *Introduction to Frustrated Magnetism*, edited by C. Lacroix, P. Mendels, and F. Mila (Springer, Berlin, 2011), Chap. 13, p. 331.
- [34] T. A. Tóth, A. M. Läuchli, F. Mila, and K. Penc, *Phys. Rev. B* **85**, 140403(R) (2012).
- [35] B. A. Ivanov and A. K. Kolezhuk, *Phys. Rev. B* **68**, 052401 (2003).
- [36] $z = 4, 6$ for the square and triangular lattices, respectively.
- [37] K. Hukushima and K. Nemoto, *J. Phys. Soc. Jpn.* **65**, 1604 (1996).
- [38] The simple mean-field approach assumes that d_i in Eq. (2) is spatially uniform, whereas sSU(3)-MC allows d_i to vary both in space and in Monte Carlo timescale, which takes account of the fluctuation other than and the quantum condensation effect referred in [41]. There, the fluctuation originating from the inter-site quantum entanglement can be replaced by the Monte Carlo averages. Particularly for the class of trivial long range order which are well approximated by the product state of the locally entangled unit [e.g., product of quadrupoles in Eq. (2)], the quantum and thermal fluctuation cannot be discriminated, and the present treatment gives a good description.
- [39] H. Kawamura and A. Yamamoto, *J. Phys. Soc. Jpn.* **76**, 073704 (2007).
- [40] S. Bhattacharjee, V. B. Shenoy, and T. Senthil, *Phys. Rev. B* **74**, 092406 (2006).
- [41] See Supplemental Material at <http://link.aps.org/supplemental/10.1103/PhysRevB.102.140401> for the details on the estimation of the low-temperature behavior and the entropy $\mathfrak{S}(T, h)$, which includes Refs. [47,48] and also for the detailed results of the ferroquadrupolar phase in the square lattice, as noted in the remarks for Fig. 3.
- [42] $J = 1/\sqrt{5}$ and $K = 2/\sqrt{5}$.
- [43] $J = -1/\sqrt{5}$ and $K = -2/\sqrt{5}$.
- [44] N. D. Mermin and H. Wagner, *Phys. Rev. Lett.* **17**, 1307 (1966).
- [45] In the present study using the semiclassical approximation, the emergent quasi-long range order is related to the topological (Kosterlitz-Thouless) transition of binding-unbinding pairs of half vortices [35]. The topological transition temperature generally falls slightly below the peak of the specific heat. However, it is not clear whether the fully quantum Hamiltonian Eq. (1) still shows such topological transition, since its possibility is excluded in the QMC study in Ref. [28] for the $h = 0$ case on the square lattice.
- [46] H. Tsujii, C. R. Rotundu, T. Ono, H. Tanaka, B. Andracka, K. Ingersent, and Y. Takano, *Phys. Rev. B* **76**, 060406(R) (2007).
- [47] H. Kawamura, *J. Phys. Soc. Jpn.* **53**, 2452 (1984).
- [48] C. L. Henley, *Phys. Rev. Lett.* **62**, 2056 (1989).